Efficiency limits of energy conversion by light-driven redox chains

Jonathan D. Schultz[a], Kelsey A. Parker[a], Michael J. Therien[a], and David N. Beratan[a,b,c*]

[a] *Department of Chemistry, Duke University, Durham, NC, 27708, USA*
[b] *Department of Physics, Duke University, Durham, NC, 27708, USA*
[c] *Department of Biochemistry, Duke University, Durham, NC, 27710, USA*

ABSTRACT

The conversion of absorbed sunlight to spatially separated electron-hole pairs is a crucial outcome of natural photosynthesis. Many organisms achieve near-unit quantum yields of charge separation (one electron-hole pair per incident photon) by dissipating as heat more than half of the light-energy that is deposited in the primary donor. Might alternative choices have been made by Nature, that would sacrifice quantum yield in favor of producing higher energy electron/hole pairs? Here, we use a multi-site electron hopping model to address the kinetic and thermodynamic compromises that can be made in electron transfer chains, with the aim of understanding Nature's choices and opportunities in bioinspired energy-converting systems. We find that if the electron-transfer coordinates are even weakly coupled to a high-frequency vibrational mode, substantial energy dissipation is *necessary* to achieve the maximum possible energy storage in an electron-transfer chain. Since high-frequency vibronic coupling is common in physiological redox cofactors, we posit that biological reaction centers have recruited a strategy to convert light-energy into redox potential with the near-optimum energy efficiency that is possible in an electron-transfer chain. Our simulations also find that charge separation in electron-transfer chains is subject to a minimum inter-cofactor separation distance, beneath which energy dissipating charge recombination is unavoidable. We find that high quantum yield and low energy dissipation can thus be realized simultaneously for multistep electron transfer if recombination pathways are uncoupled from high-frequency vibrations and if the cofactors are held at small-to-intermediate

distances apart (ca. 3 to 8 Å edge-to-edge). Our analysis informs the design of bioinspired light-harvesting structures that may exceed 60% energy efficiency, as opposed to the ~30% efficiency achieved in natural photosynthesis.

INTRODUCTION

A vital stage of oxygenic and anoxygenic photosynthesis is the conversion of localized electronic excitons into spatially disparate electron-hole pairs.[1-7] This critical charge separation (CS) is performed in photosynthetic organisms with a series of sequential electron-transfer (ET) reactions that achieve long-range CS with near-unit quantum yield.[2,8,9] The ET dynamics in reaction centers (RCs) of purple bacteria, for example, proceed from a chlorophyll special pair electronically excited state through a sequence of intermediate CS states involving a chain of chlorophyll, pheophytin, and quinone cofactors that are bound to the RC protein.[1,2,10-12] The sequence is completed by the formation of a terminal CS state (with an electron on the secondary quinone and hole on the special pair[1,2,9]); the energy of this state compared to the special pair exciton defines the amount of energy transduced by the RC.

The quantum yield of long-range (several nanometers) CS achieved by natural photosynthetic RCs is enviable from the standpoint of bioinspired materials design, but the high quantum yield comes at a thermodynamic cost: *more than one-half of the special pair's electronic excitation energy is dissipated in forming the terminal CS state*.[1,2,13] Previous studies[13-16] used Marcus-like frameworks[14,17-19] to explain why biological RCs may have evolved the large fractional energy dissipation strategy for energy conversion. Temperature-dependence studies[1,2,13,20-24] of photoinduced and thermal charge recombination (CR) reactions in purple bacteria RCs, for example, found that several of the forward ET steps (those that separate the electron and hole by increasingly larger distances) have nearly zero activation free energy, which leaves the energy

dissipating CR reactions deeply in the Marcus-inverted region.[14,16,25] The resulting energy landscape effectively suppresses energy-wasting CR pathways by strongly favoring forward ET for each intermediate CS state. Such a picture is congruent with observations that the rates of forward ET in the purple bacteria RC exceed the corresponding CR rates by several orders of magnitude.[2,15,16,25]

While the combination of barrierless forward ET and Marcus-inverted CR may enable high CS quantum yields in ET chain architectures, activationless ET requires that the driving force ($-\Delta G^{(0)}$) match the reorganization energy (λ). Thus, each forward ET step is accompanied by a substantial dissipation of free energy (typical[26-29] λ values are hundreds of meV). Energy harvesting schemes that rely on a series of sequential ET steps therefore face an intrinsic compromise between maximizing the quantum yield (achieved in natural systems through $-\Delta G^{(0)} \approx \lambda$ at each step) and minimizing the net free energy dissipated (minimizing $-\Delta G^{(0)}$ at each step).[30,31] Understanding Nature's logic in managing the tradeoff between the quantum yield for charge separation and the energy stored in the terminal CS state may provide insights into evolutionary pressures on biological energy-conversion machines and inform bioinspired energy transducing strategies.[32-34] Indeed, lessons drawn from natural photosynthetic structures are already being used to guide endeavors toward artificial photosynthesis,[35-39] and a number of impressive synthetic multi-step ET architectures have been realized.[39-49] Though much progress has been made in the direction of biomimetic and bioinspired charge separation,[37,38] much focus has been on the quantum yield of CS,[45-47] with less attention paid to the redox energy stored in the terminal ET state.

Here, we explore how the optimum energy efficiency (η) may be realized in multisite ET chains through the interplay between the quantum yield and ET product state energy. While classical Marcus theory predicts accessible energy efficiencies ($\eta > 60\%$) for such redox chains

that are significantly higher than those found in bacterial RCs ($\eta < 40\%$), we show that coupling the ET dynamics to a quantum vibrational mode disproportionately enhances CR rates[50-54] and, in turn, decreases η and changes the optimal structural and energetic requirements (e.g., inter-cofactor spacings and driving forces) toward conditions commonly observed in nature.[1,2,13,20-23] Though our model represents an idealized design, our findings suggest that the substantial free energy dissipation in bacterial RCs may be a result of ET coupling to high-frequency modes. Extrapolating our findings beyond the interpretation of the forces at play in natural systems, we describe strategies that could be used to maximize the energy efficiency of synthetic light-driven ET hopping chains. Most notably, we predict that decoupling the ET dynamics from intramolecular vibrations could enable the assembly of energy transducing redox chains with higher efficiencies (η values) while maintaining near-unit CS quantum yields.

METHODS

Theoretical model

The energetic landscape of bacterial photosynthetic RCs is approximated with a primary electron donor and three electron acceptors,[1,2,15] and such tetrads have been studied experimentally.[38,46,48,49,55-57] The model redox chain offers a convenient framework in which to explore how the captured free energy depends on the redox potential landscape. Figure 1a shows the energy ordering of the six relevant electronic states: the ground state ($\mathbf{DA_1A_2A_3}$), the locally excited singlet state ($\mathbf{^1D^*A_1A_2A_3}$), three CS states ($\mathbf{D^+A_1^-A_2A_3} \rightleftharpoons \mathbf{D^+A_1A_2^-A_3} \rightleftharpoons \mathbf{D^+A_1A_2A_3^-}$), and a sink (**s**) that acts as an irreversible trap state coupled to the terminal acceptor. The dynamics from the $\mathbf{^1D^*A_1A_2A_3}$ state proceed through a combination of competing steps that include radiative and nonradiative decay, forward electron transfer (FET), back electron transfer (BET), and CR as

indicated in Figure 1. We assume that there is no direct formation of CS states from the ground state (the CR paths denoted by the green arrows in Figure 1a are unidirectional).

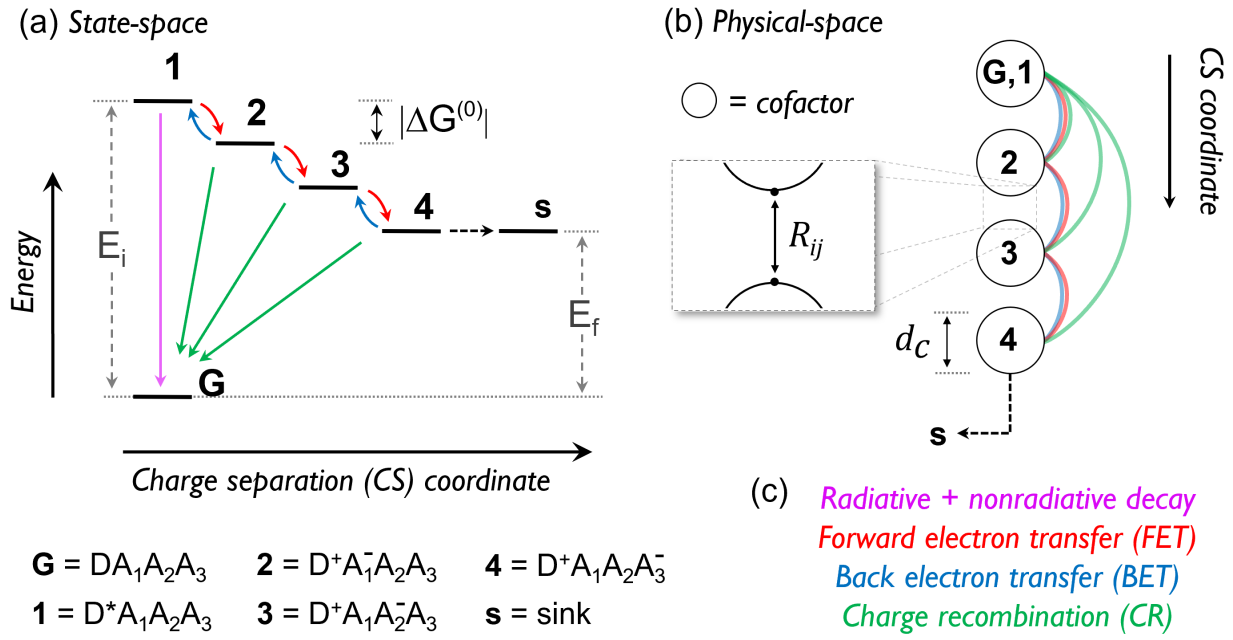

Figure 1. (a) Energy level diagram for the model ET chain studied in this work. (b) The model includes six electronic states (G, 1, 2, 3, 4, and the sink) that span four cofactor sites linearly connected in space. Neighboring cofactors (i and $i\pm1$) are separated by distance R_{ij}. (c) Color-coding for the dynamical processes considered in the model, as indicated with arrows and arcs in (a) and (b), respectively.

The energy conversion performance of the ET chain in Figure 1a depends both on the quantum yield of electrons to arrive on the sink (the terminal CS product) and the fraction of the ^{1}**D*** energy preserved through the CS. We define the quantum yield of CS (φ_{CS}) as

$$\varphi_{CS} = P_s(t \to \infty), \qquad \text{eq 1}$$

where $P_s(t\to\infty)$ is the long-time (equilibrium) population of the sink state. We define the energy efficiency (η) as

$$\eta = P_s(t \to \infty)\frac{E_f}{E_i}\,, \qquad \text{eq 2}$$

following a recent study of Ivanov and coworkers.[31] E_i is the energy of the photoexcited state (^{1}**D*A$_1$A$_2$A$_3$**) above the ground state (**DA$_1$A$_2$A$_3$**), and E_f is the energy of the sink.

We describe the single-particle ET dynamics of the chain in Figure 1 using a kinetic master equation, which is provided in eq S1 of the Supporting Information (SI). The term k_{ij} represents the rate constant for population transfer between states i and j (as defined in Figure 1a). We calculate all ET rates (FET, BET, and CR) using the semiclassical rate expression[50-54,58]

$$k_{ij} = \frac{2\pi^{3/2}}{\hbar\sqrt{\lambda_c \kappa_b T}}\left|V_{ij}\right|^2 e^{-S}\sum_n \frac{S^n}{n!}\, e^{-\frac{\left(\Delta G_{ij}^{(0)}+\lambda_c+n\hbar\omega\right)^2}{4\lambda_c k_b T}}, \qquad \text{eq 3}$$

where $-\Delta G_{ij}$ is the driving force, V_{ij} is the electronic coupling, λ_c is the classical reorganization energy, T is the temperature, $\hbar$ is the reduced Planck constant, and k_b is the Boltzmann constant. Here, we define $-\Delta G_{ij}^{(0)}$ as the driving force for FET (thus, $\Delta G_{ij}^{(0)}$ is the driving force for BET). The classical reorganization energy accounts for all contributions from classical modes (inner- or outer-sphere). A quantum vibrational reorganization energy (λ_{vq}) from high-frequency modes ($\hbar\omega \gg k_bT$) is also included in eq 3, where the Huang-Rhys factor (S) establishes coupling of ET to a single effective mode with frequency $\hbar\omega$ ($S = \lambda_{vq}/\hbar\omega$).[29,51,52,54,58,59] The total reorganization energy is $\lambda_c + \lambda_{vq}$. In the limit of $S \to 0$, eq 3 becomes the nonadiabatic rate associated with classical (high-temperature) Marcus theory.[18,19]

The states in Figure 1a each represent a cofactor orbital delocalized across N atoms. Figure 1b maps the state numbers to cofactor sites. We use Hopfield's one-dimensional square barrier approximation[60-62] to approximate the distance-dependent electronic coupling:

$$V_{ij} = \frac{V_0}{\sqrt{N_i N_j}} e^{-\frac{\beta R_{ij}}{2}}, \qquad \text{eq 4}$$

where R_{ij} is the shortest atom-to-atom distance between the the donor/acceptor states *i* and *j*, V_0 is the reference electronic coupling, β is the wavefunction tunneling decay parameter,[62-66] and N_i and N_j are the numbers of atoms over which the states *i* and *j* are delocalized (we assume $N_i = N_j$). The value of β can be varied to reflect the nature of the medium through which the electron tunneling occurs.[64-69]

Model parameterization

We parameterize the model ET chain using values representative of biological systems (see Table 1). We fix E_i = 1.4 eV to mimic the approximate excited-state energy of the special pair in *Rb. sphaeroides*[1,2,5,13,24,70] (the value of E_i relative to $-\Delta G^{(0)}$ is the critical parameter). We set β = 1.4 $Å^{-1}$, which is typical for tunneling decays through an alpha-helical protein[5,20,60,64-68,71] and is consistent with previous studies[5] of bacterial RCs (Figure S10 provides results of simulations with different β values). Following Hopfield's approach,[60] V_0 = 2.7 eV. We set N = 20 for the results discussed in the main text which, assuming chlorin-based cofactors, yields a reasonable value of ~ 9.1 Å for the cofactor diameter (d_c). In the kinetic master equation, we fixed $k_{1G} = 10^9$ s^{-1} to approximate the sum of the radiative and non-radiative decay rates from the special pair (see the SI for further discussion).[2,70] Also, *Rb. sphaeroides* is an example of a type II RC, which is defined by a mobile secondary quinone that acts as the terminal electron acceptor.[8,11,21] Dissociation of the secondary quinone to its unbound state, which occurs on the timescale of 10^{-2} to 10^{-1} seconds in *Rb. sphaeroides*, yields a sink-like effect by shutting down CR. In our simulations, we set $k_{4s} = 10^2$ s^{-1} to mimic quinone dissociation and, for simplicity, consider the process to be irreversible.

We modeled chains with equal distances between neighboring cofactors (i.e., $R_{12} = R_{23} = R_{34} = R$, as shown in Figure S5 and eq S6). We varied R to cover the inter-cofactor spacings found in biological ET proteins (spacings between ~3 and 14 Å are most commonly observed).[5,6,72] We also set the ET driving force for neighboring cofactors to be equal: $-\Delta G_{12}^{(0)} = -\Delta G_{23}^{(0)} = -\Delta G_{34}^{(0)} = -\Delta G^{(0)}$. The free energy captured when the electron arrives at the sink is thus $E_f = E_i + 3\Delta G^{(0)}$. These restrictions on $-\Delta G^{(0)}$ and ΔR cause: $k_{12} = k_{23} = k_{34} = k_{FET}$ and $k_{21} = k_{32} = k_{43} = k_{BET}$ (from detailed balance, the ratio of forward and back ET rates differ by $\exp[-\Delta G^{(0)}/k_bT]$). Note that rates of electron-hole CR (i.e., k_{2G}, k_{3G}, and k_{4G}) are not equal, and this fact is important in our assessments of efficiencies.

The value of λ_c depends on the redox cofactors and the surrounding medium.[25,73-75] The interplay of energy capture and dissipation by the redox chain depends on the *relative scales* of $-\Delta G^{(0)}$ and λ_c. Thus, we vary $-\Delta G^{(0)}$ and fix $\lambda_c = 0.3$ eV, which is typical of values in the low dielectric environment of the RC.[1,5,31,76] When $\lambda_c = 0.3$ eV, the values of $-\Delta G^{(0)} = 0$ and 0.467 eV define two important limits: $-\Delta G^{(0)} = 0$ corresponds to zero energy dissipation ($E_f/E_i = 1$), while $-\Delta G^{(0)} = 0.467$ eV corresponds to 100% energy dissipation ($E_f/E_i = 0$).

Table 1. Parameters used in the ET chain model. Brackets denote parameters that we scanned over a range of values (bracket format is as follows: [minimum value; maximum value; total number of evenly spaced values between the minimum and maximum values]).

Parameter	Unit	Value(s)	References
E_i	eV	1.4	1,2,5,13,24,70
λ_c	eV	0.3	1,5,13,76
$-\Delta G^{(0)}$	eV	[0.467; 0; 149]	-
$\hbar\omega$	eV	0.15	13,22,50-52,59,77,78
S	-	0, 0.25, 1, 2, 3, 4	50-52,59,77
n	-	100	-
V_0	eV	2.7	60
R	Å	[0; 15; 149]	5,6,72
β	$Å^{-1}$	1.0, 1.4, 2	5,20,60,64-68,71
N	-	6, 20, 100	-

k_{4s}	s^{-1}	10^2, 10^4, 10^6	11,21
k_{1G}	s^{-1}	10^9	2,70
k_bT	eV	0.025	-

Population dynamics

Each combination of the parameters indicated in Table 1 produces a different rate matrix that describes that system's kinetics. We launch each kinetic simulation with the system in the photoexcited ^{1}**D*A$_1$A$_2$A$_3$** state at t = 0; at later times we calculate the population dynamics analytically using a first-order kinetic master equation.[79] After the system has reached equilibrium, we compute φ_{CS} and η. Further details of the model, including example dynamics (Figure S2), are provided in the SI.

RESULTS AND DISCUSSION

Energy efficiency in the classical Marcus-like rate limit

The redox potentials of the cofactors and the spacings between them exert exponential control over the kinetic constants in bacterial RCs.[6,15,32] We therefore simulate the ET chain dynamics as a function of $-\Delta G^{(0)}$ and R, which allows us to assess how the balance of yield and energy capture varies with the system geometry and free energy landscape. Figure 2a shows the energy efficiency of the chain as a function of the ($-\Delta G^{(0)}$, R) parameter space (Figures S3a and S3b show the corresponding quantum yield and energy ratio, respectively). Notably, barrierless FET ($-\Delta G^{(0)} = \lambda_c = 0.3$ eV) does not produce high ET chain energy efficiency (Figure 2a). Rather, the maximum values of η (abbreviated herein as η_{max}) are found near $-\Delta G^{(0)} = 0.16$ eV for all R < ca. 6 Å. For example, $\eta \approx 0.63$ for $-\Delta G^{(0)} \sim 0.16$ eV and R = 3.5 Å (approximately van der Waals contact[33]). Examining the inter-state rate constants (e.g., Figure 2b), we find that high η at small $-\Delta G^{(0)}$ is possible because of the Marcus-inverted nature of the CR pathways (Figure 2c). This observation

aligns with experimentally supported hypotheses[1,14-16,54,80] that high-yield CS in photosynthetic RCs is afforded (at least in part) by the placement of CR pathways in the Marcus inverted region.

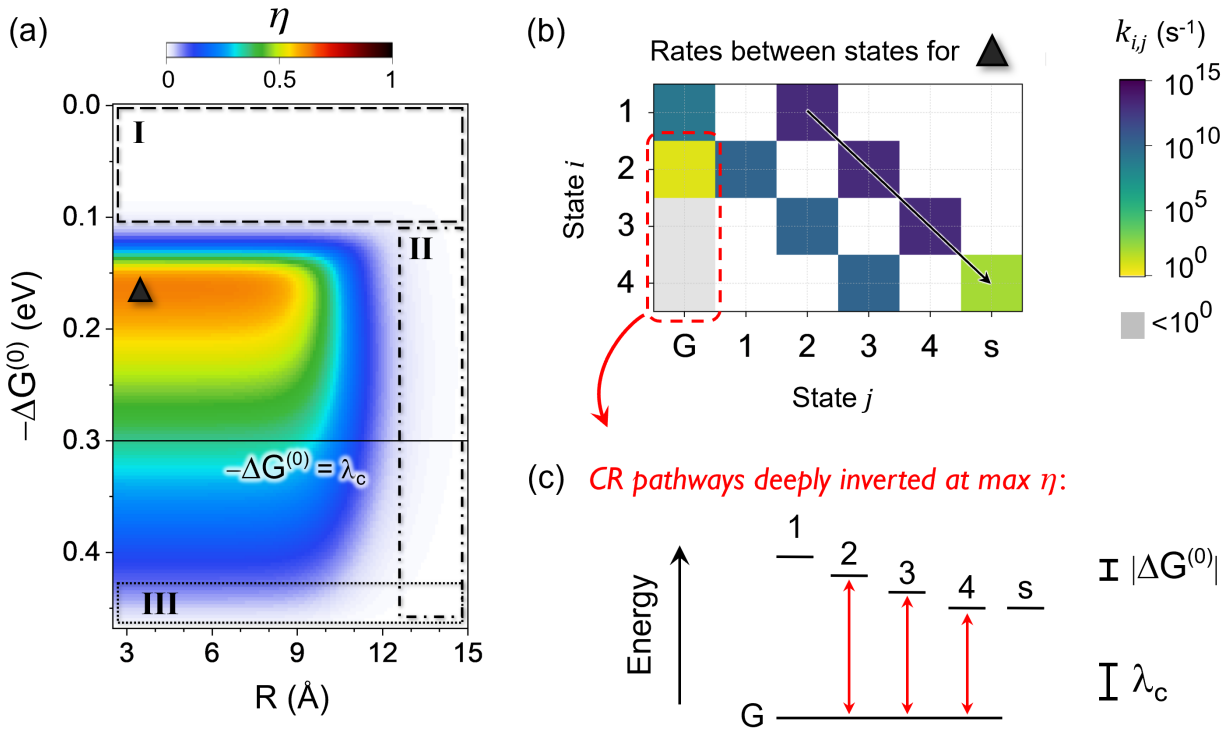

Figure 2. (a) Energy conversion efficiency of the ET chain as a function of driving force and inter-cofactor spacing in the classical Marcus framework. The condition of barrierless FET ($-\Delta G^{(0)} = \lambda_c$) is indicated by a solid horizontal line. The approximate boundaries of three regions with $\eta \rightarrow 0$ are labeled with dashes (I), dashes and dots (II), and dots (III). (b) A matrix representation of the rates between the electronic states of the ET chain at the conditions for $\eta \approx \eta_{max}$, as denoted by the triangle in (a). Figure S4 shows additional matrix representations. (c) Chains with near-maximum energy efficiency feature deeply inverted CR pathways (the energy gaps, driving forces, and solvent reorganization energies are drawn approximately to scale).

We observe several regions of the parameter space (labeled with Roman numerals in Figure 2a) that consistently give rise to low energy efficiency for the ET chain. Regions I and II (characterized by $-\Delta G^{(0)} < 0.11$ eV and $R \gtrsim 12$ Å, respectively) produce $\eta \approx 0$ due to low φ_{CS} (Figure S3a). In region I, φ_{CS} approaches zero because k_{FET} is not sufficiently fast to outweigh k_{BET} and to generate forward CS (for example, see Figure S4b,c). Thus, energy is lost in region I to decay of the primary donor excited state (^{1}**D*A$_1$A$_2$A$_3$**). Decay of ^{1}**D*A$_1$A$_2$A$_3$** also drives low φ_{CS}

in region II (Figure S4c,e,h), since all ET rates in the chain drop below k_{1G} when the inter-cofactor separation becomes too large (> ca. 10 Å). Finally, Figure S3b shows that η approaches zero in region III ($-\Delta G^{(0)} \gtrsim 0.43$ eV) due to substantial energy dissipation (low E_f/E_i). Figure 3a summarizes the dominant reasons for low η values within the ($-\Delta G^{(0)}$, R) parameter space in the limit of classical Marcus theory.

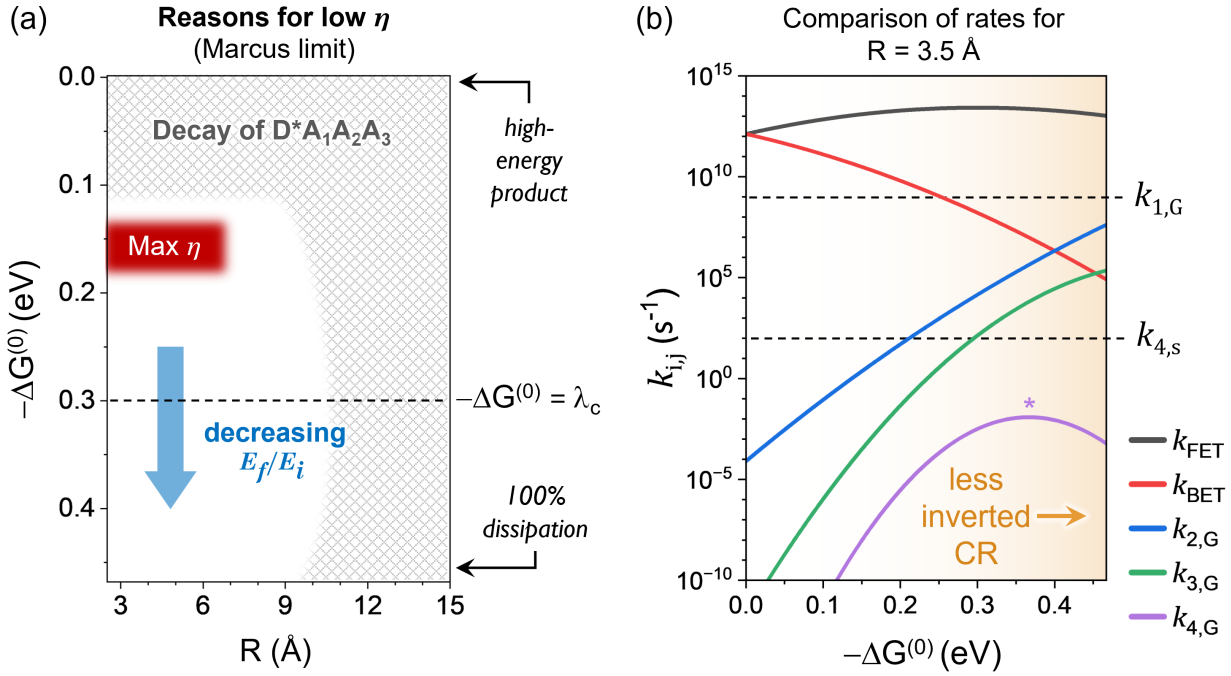

Figure 3. (a) Qualitative summary of the factors that contribute to low η within the parameter space of driving force and inter-cofactor spacing. (b) ET rates as a function of driving force with R = 3.5 Å. The lavender asterisk marks the point of barrierless CR from the fourth cofactor ($\mathbf{D^+A_1A_2A_3^-} \rightarrow \mathbf{DA_1A_2A_3}$).

Along with dissipating more energy, increasing $-\Delta G^{(0)}$ causes the CR pathways to become less inverted (faster rates). For example, Figure 3b shows that for Marcus-inverted FET ($-\Delta G^{(0)} > 0.3$ eV) and R = 3.5 Å, the rates of CR from the primary ($\mathbf{D^+A_1^-A_2A_3} \rightarrow \mathbf{DA_1A_2A_3}$) and secondary ($\mathbf{D^+A_1A_2^-A_3} \rightarrow \mathbf{DA_1A_2A_3}$) CS states both exceed k_{4s} and approach k_{BET}. Also, CR from the tertiary CS state ($\mathbf{D^+A_1A_2A_3^-} \rightarrow \mathbf{DA_1A_2A_3}$) becomes activationless when $-\Delta G^{(0)} = 0.367$ eV (purple asterisk). While CS still outcompetes CR for all $-\Delta G^{(0)}$ in Figure 3b, we find that ET chains with

smaller cofactor diameters (Figure S9c) or slower wavefunction decay (Figure S10c) are susceptible to fast CR reactions and low η when $-\Delta G^{(0)}$ is large and R is small.

The rates of FET, BET, and CR all depend on R through the distance dependence of V_{ij}, as we neglect the distance dependence of λ. One may therefore ask why the efficiencies of ET chains with large R are not decreased by CR. ET rates between neighboring cofactors (i.e., k_{FET}, k_{BET}, and k_{2G}) decay exponentially with R (eqs 3 and 4). However, direct CR from the $\mathbf{D^+A_1A_2^-A_3}$ and $\mathbf{D^+A_1A_2A_3^-}$ states back to $\mathbf{DA_1A_2A_3}$ (indirect recombination via sequential BET and CR from $\mathbf{D^+A_1^-A_2A_3}$ is unfavorable due to the uphill free energy ramp) requires the electron to hop over multiple factors of R (two and three, respectively, as illustrated in Figure S5a). The rates of CR from states that are multiple cofactor sites away from the primary donor (k_{3G} and k_{4G} here) therefore possess stronger distance dependencies than the nearest-neighbor ET rates (Figure S5b). In turn, the net influence of CR on the CS yield is largest for small R, which aligns with earlier ideas of Feher et al.[2] and Rutherford et al.[15] It follows that as the distance between the electron and hole grows, FET steps are increasingly favored over CR.

In agreement with previous studies,[2,15,16,80] we find that suppression of CR pathways via the Marcus-inverted effect can support high-yield CS in ET chains. However, our simulations suggest that high energy conversion efficiencies (η > 60%) should be accessible at significantly lower driving forces ($-\Delta G^{(0)} \approx \lambda_c/2$) than are typically observed[1,2,24] in bacterial RCs ($-\Delta G^{(0)} \approx \lambda_c$). As the slowing of rates by Marcus-inverted effects is well-known to be softened by coupling of the ET to high-frequency nuclear vibrations,[50,52-54,81] introducing such modes may well change the influence of CR pathways on network efficiencies. We next explore the performance of ET chains with the dynamics coupled to a high frequency quantum vibration.

Influence of high frequency modes on energy efficiency

The rate of ET in the Marcus inverted regime is known to be accelerated by coupling to high-frequency vibrational modes.[52-54,81] Figure 4a shows the energy efficiency of the ET chain for the same ($-\Delta G^{(0)}$, R) parameter space spanned in Figure 2a, but with one effective high-frequency mode (with typical values of $\hbar\omega = 0.15$ eV ≈ 1210 cm^{-1} and S = 2, or $\lambda_{vq} = 0.3$ eV) coupled to all the ET pathways. Figures S6 and S7 show the results of simulations with other values of the Huang-Rhys factor. We find that η is very sensitive to the strength of the high-frequency vibronic coupling, especially at small forward driving forces and small inter-cofactor spacings. For example, whereas $\eta \approx 0$ in the region bounded by the gray dashed box in Figure 4a, the classical Marcus framework predicts $\eta > 60\%$ in this region (Figure 2a). Figure 4b illustrates the inter-state rates for the conditions denoted by the triangle in Figure 4a (conditions that correspond to η_{max} in the Marcus limit). Compared to the rates predicted by the classical Marcus equation (Figure 2b), Figure 4b features a substantial increase in the CR rates, especially k_{2G} and k_{3G} (Figure 4c). Therefore, by weakening the inverted rate effects on the CR pathways, coupling to a high-frequency quantum mode precludes the high η at small $-\Delta G^{(0)}$ that is possible for ET chains in the absence of electron-vibration coupling to a high-frequency mode (Figure 2a).

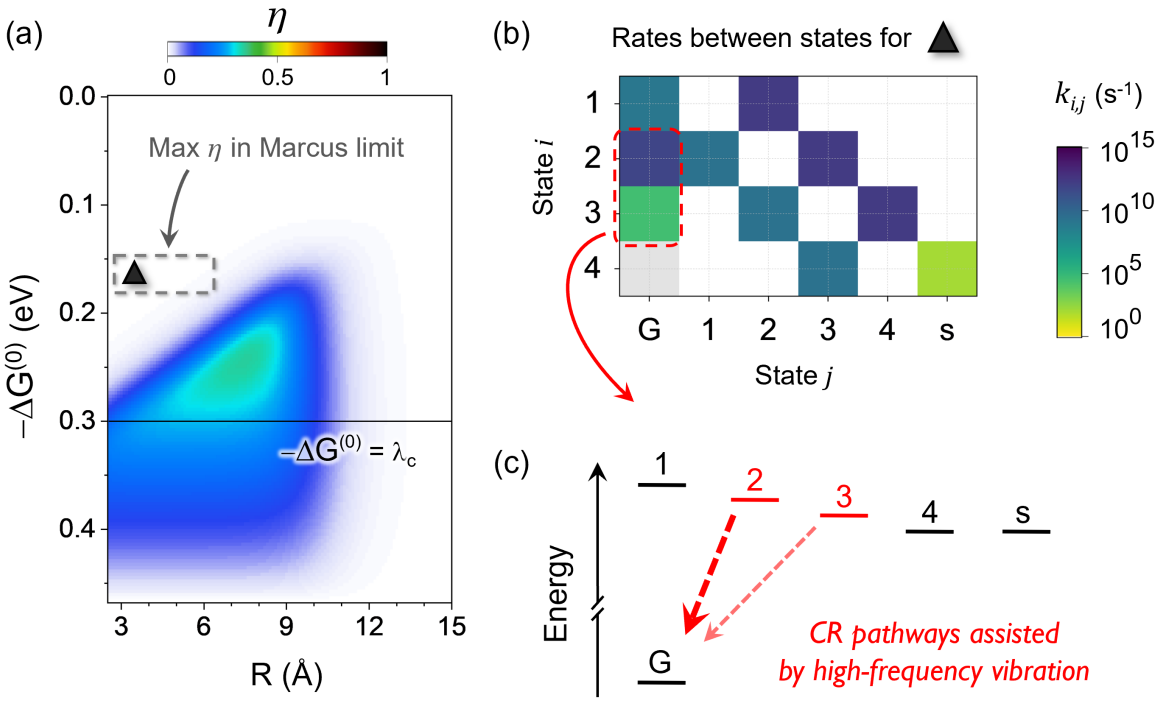

Figure 4. (a) Energy conversion efficiency of the ET chain as a function of forward driving force and inter-cofactor spacing. S = 2 for the high-frequency quantum mode ($\hbar\omega$ = 0.15 eV ≈ 1210 cm^{-1}), so λ_{vq} = 0.3 eV. A dashed gray box indicates the approximate region of the parameter space that yields highest η in the limit of classical Marcus theory. (b) A matrix representation of the rates between the electronic states of the ET chain at the conditions denoted by the triangle symbol in (a). (c) A diagram for the dominant decay pathways within the regions of the parameter space near the triangle in (a).

Figure 5a shows how the maximum possible energy efficiency, η_{max}, of the ET chain depends on the Huang-Rhys factor (S = $\lambda_{vq}/\hbar\omega$). Notably, η_{max} decreases linearly with increasing S, and η_{max} of the fit equals zero near S = 4.3 (corresponding to λ_{vq} = 0.645 eV for $\hbar\omega$ = 0.15 eV). The strength of the coupling to a high-frequency vibration is therefore a key factor that determines the energy efficiency for multi-step ET hopping (see Figure S7 for related discussion). Figure 5b also shows that changing S skews the physical parameters for ET chains that realize efficiencies closer to η_{max}: as S increases, η_{max} occurs at larger -$\Delta G^{(0)}$ values (left axis of Figure 5b) and generally

larger R values (right axis of Figure 5b), although R for η_{max} decreases slowly as S increases beyond 0.75.

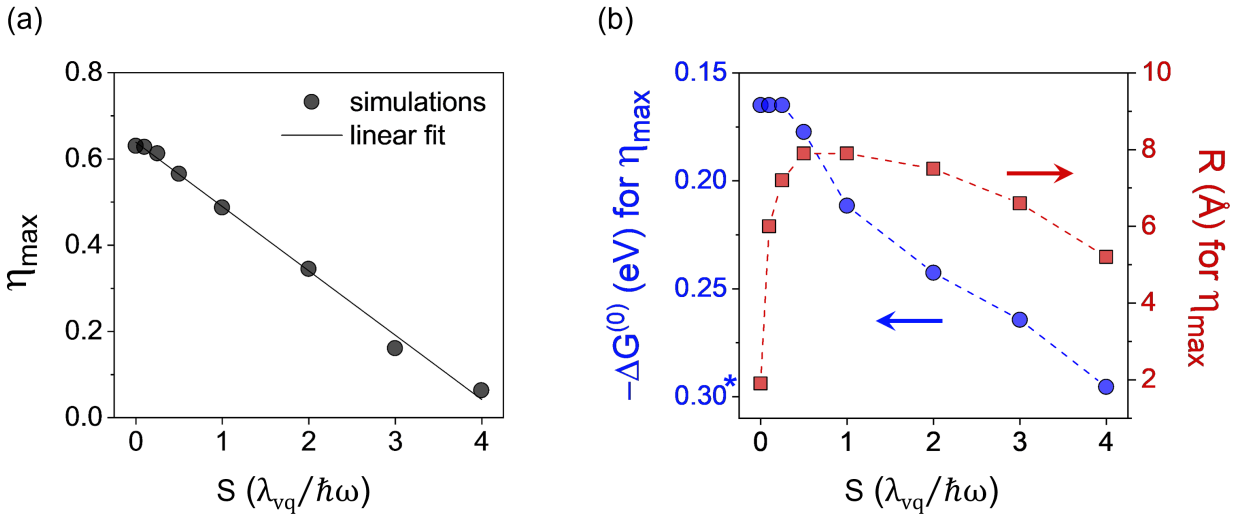

Figure 5. (a) Maximum energy efficiency as a function of Huang-Rhys factor. The x-intercept of the linear fit (R^2 = 0.995) is S = 4.28 ± 0.09. (b) Values of $-\Delta G^{(0)}$ (blue, left axis) and R (maroon, right axis) that are required for η_{max}. An asterisk (left axis) marks the condition of $-\Delta G^{(0)} = \lambda_c$.

Compared to the detailed structure of reaction centers found in nature, the theoretical model and the range of conditions explored in this study represent idealized scenarios. Still, as Figure 6 indicates, we find qualitative parallels between our findings and observations made in studies of bacterial RCs. In contrast to the conditions for optimal η in the limit of Marcus theory (small $-\Delta G^{(0)}$ and R near van der Waals contact), increasing the coupling of the ET dynamics to a high-frequency mode pushes the conditions for η_{max} toward values of $-\Delta G^{(0)}$ and R that are more reflective of the those found[1,2,5-7,13,20-23,72] in bacterial RCs (i.e., $-\Delta G^{(0)} \approx \lambda_c$ and R frequently several Å greater than van der Waals contact). The connection between bacterial RC function and multi-step hopping coupled to high-frequency modes is widely recognized,[1,2,5,13,22,59] and some studies[13,22,25] posit that vibrations may limit the extent to which natural systems can suppress CR reactions via the Marcus-inverted effect. Building on these previous studies, our results find that

the high-frequency component of the reorganization energy in multi-step ET chains: (i) defines the balance between CS quantum yield and the energy of the terminal electron/hole pair that produces optimal free energy capture; (ii) provides an explanation for why the distances and driving forces for η_{max} predicted by classical Marcus theory are infrequently recruited[72] in biological systems (Figure 6).

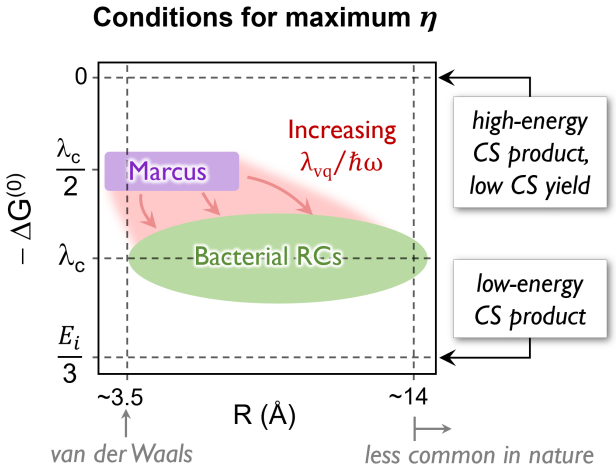

Figure 6. A schematic summary of the conditions required to achieve maximum energy efficiency from the ET chain architecture. Coupling the ET processes to a high-frequency vibrational mode pushes the conditions for optimal η away from the Marcus limit (purple shaded region) and toward those more commonly observed in bacterial RCs[1,2,5-7,13,20-23,72] (i.e., $-\Delta G^{(0)} \approx \lambda_c$ and R values often several Å larger than van der Waals contact, as portrayed by the green shaded region).

The physiological influence of high-frequency cofactor vibrations on ET kinetics is well-documented.[13,22,59,78] For example, experimental observations of non-Arrhenius temperature dependencies led Bixon and Jortner to suggest[59] that S ~ 0.5 to 1 for the CR pathways in *Rb. sphaeroides* RCs. Setting S = 1 for the model ET chain studied here constrains the energy conversion to $\eta_{max} < 0.45$ (Figure S6b). Thus, despite dissipating of over half of the primary donor's energy, bacterial photosynthetic RCs may very well operate near their maximum energy efficiency. Unless the high-frequency vibronic coupling can be reduced (*vide infra*), our model

predicts that natural systems are unable to sacrifice quantum yield in favor of producing higher energy electron/hole pairs.

On the "robustness" of transport in ET chains

For ET chains in which the classical Marcus rate equation is valid, we find that high η is achievable at low $-\Delta G^{(0)}$ and small R values (Figure 2a). Taking a closer look at the contribution of the CS quantum yield to η, we find that a wide range of $-\Delta G^{(0)}$ and R values produce near-unit quantum yield ($\varphi_{CS} > 0.95$ within the entire area enclosed by gray dashes in Figure 7a). In contrast, Figure 7b shows that the $-\Delta G^{(0)}$ and R dependencies of φ_{CS} for a single-hop ET dyad (two cofactors) are sharply peaked near $-\Delta G^{(0)} \approx 0.39$ eV and R ≈ 10.5 Å. Previous studies[15,32,34,72,82] discussed the propensity of ET chains, including the photosystem I RC,[7] to tolerate changes in the characteristic parameters of Marcus theory. In line with these earlier notions of tolerance, our findings indicate that robustness of φ_{CS} to changes in $-\Delta G^{(0)}$ and R is a unique feature of multi-step hopping electron transport.

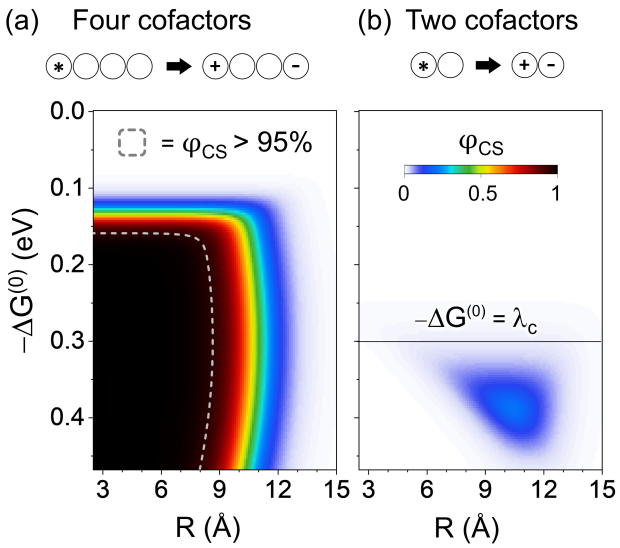

Figure 7. Quantum yield of CS for the (a) multi-hop ET chain (four cofactors) and (b) a single-hop ET dyad (two cofactors) calculated with identical model parameters. The area enclosed by the dashed gray shape in (a) indicates all regions of the parameter space with $\varphi_{CS} > 0.95$.

Principles for the design of efficient ET chains

Multi-step ET chains provide a motif for separating electrons and holes over large distances with high quantum yield (as exemplified by Figure 7). The energy efficiency analysis described here highlights strategies to optimize free energy transduction in light-driven multi-step ET hopping chains, depending on the nature of the vibronic coupling (whether to high- or low-frequency modes). Our principal finding is that achieving the maximum energy conversion efficiency of an ET chain system *requires* significant energy dissipation (upwards of 50%) if the ET dynamics are coupled (even weakly) to a high-frequency vibrational mode. When the electron-vibration coupling is significant, vibrational excited states of $\mathbf{DA_1A_2A_3}$ provide efficient deactivation channels via CR, especially when the intercofactor spacings are small. Thus, decoupling the ET reactions from high-frequency vibrational modes ($S \rightarrow 0$) is an effective way to reduce energy dissipation in ET chains while maintaining high quantum yield (i.e., via the Marcus inverted effect).

Considering both the incidence of deviations from classical Marcus inverted behavior reported in the literature[54,58,83,84] and the known proclivity of classical Marcus theory to underestimate rates of highly exergonic ET reactions,[85-87] decoupling ET processes from intramolecular vibrations is not a simple design challenge to realize. However, some ET reactions do fit the classical Marcus free energy behavior. For example, Gray and coworkers found a Gaussian free-energy dependence for photoinduced CS rates in iridium-based donor-acceptor complexes.[88] A similar dependence was also been reported for the rates[89] and yields[90] of photoinduced CS in organic semiconductor blends. The inner-sphere reorganization energy generally depends on factors including molecular size, symmetry, and electronic structure (e.g., delocalization).[26-28,91-94] Thus, synthetic strategies may enable the minimization of the inner-sphere contribution to λ_{vq}. For example, Gray and

coworkers demonstrated the modest tuning of porphyrin inner-sphere reorganization energies by changing substituents.[26] Chou and coworkers[92] found significant symmetry effects on the computed inner-sphere reorganization energies for cyanine dyes and substituted D-A model systems. However, to boost the energy efficiency of ET chains by synthetically minimizing high-frequency inner-sphere reorganization energies, care must be taken to avoid influencing other factors governing the overall ET chain function.[95]

Additional strategies exist to improve the efficiency of ET networks. For example, increasing the rate of ET to the sink will reduce the probability of CR. In fact, simply increasing k_{4s} to 10^6 s^{-1} yields a maximum η of 0.79 (compared to η ~ 0.63 in Figure 2a, where $k_{4s} = 10^2$ s^{-1}), thanks to the increased quantum yield at low forward driving forces (Figure S8). The performance of a light-driven ET network may also be tuned by altering the size of the cofactors (more specifically, the delocalization length of the orbitals participating in ET) and the distance decay of the electron tunneling interactions. While increased cofactor delocalization typically reduces the cofactor-to-cofactor couplings (slowing both CS and CR), delocalization can also disproportionately increase the CR distances from the $\mathbf{D^+A_1A_2^-A_3}$ and $\mathbf{D^+A_1A_2A_3^-}$ states. As such, we find that increasing cofactor size boosts the favorability of FET over CR and permits access to high η values at small R (Figure S9). Moreover, slowing the rate of tunneling decay with distance through the bridging medium (i.e., decreasing β) increases the favorability of CR over FET and leads to η = 0 for small R values (Figure S10).

The influence of inter-cofactor distances on ET rates has been explored extensively in the context of bacterial RCs.[5,6,72] While short edge-to-edge distances (less than ca. 14 Å) are generally presumed to improve the efficiency of ET chains,[7,32,33] we find cases where distances that are too short can shut down CS at large forward driving forces (for example, R < 4.5 Å for chains with β

= 1 $Å^{-1}$, as shown in Figure S10). We attribute this finding, which is exacerbated by including coupling to high-frequency modes, to the tendency of CR rates to be disproportionately enhanced (compared to CS rates) at smaller cofactor-cofactor distances (Figure S5b). In the context of energy transfer, a minimum of ca. 5 Å separation between the cofactors within the photosynthetic antennae was shown[96] to be crucial to avoid energy loss via fluorescence quenching. Consequently, the avoidance of fluorescence quenching has been hypothesized[34,96,97] to be an evolutionary constraint on the architecture of natural light-harvesting structures. Our findings suggest that the high prevalence[5,72] of edge-to-edge distances between RC cofactors that are several Å above van der Waals contact may evince an analogous evolutionary pressure to avoid CR pathways that are particularly influential at smaller inter-cofactor distances. We therefore suggest that effective synthetic ET chains will need to follow similar logic by establishing short, but not too short, distances between charge hopping stations.

CONCLUSIONS

Electron transport chains face a trade-off between disabling CR channels to maximize the quantum yield of CS and funneling as much of the initial excited state energy as possible into the terminal electron-hole pair. Motivated by early hypotheses surrounding this trade-off, our simulations of stepwise ET kinetics in linear redox chains reveal the salient system properties that determine optimal performance. First, we identified a strong sensitivity of redox chain energy conversion efficiency to vibronic coupling to high-frequency modes. In contrast to the low driving force ($-\Delta G^{(0)} \approx \lambda_c/2$) that classical Marcus theory predicts to produce the maximum efficiency of an ET chain, even weak coupling to high-frequency modes pushes the conditions for optimal energy efficiency closer to $-\Delta G^{(0)} \approx \lambda_c$ (a high energy-cost scenario that is more nearly congruent with natural systems[1,2,5-7,13,20-23,72]). Second, we showed quantitatively that the quantum yield of

multi-step hopping in ET chains exhibits a robustness to changes in driving force and inter-cofactor separation. Finally, we found a threshold for inter-cofactor distances beneath which CR pathways inevitably dominate (even if they are slowed maximally by the Marcus-inverted effect), leading to low charge separation efficiencies. The existence of such a threshold may explain the high incidence of cofactor spacings that are several Å beyond van der Waals distances in biological charge separation structures.[72]

Regarding Nature's options in balancing quantum yield versus the energy of the terminal charge separated state, our findings indicate that the balance is set critically by the strength of the vibronic coupling to high-frequency modes (likely those of the biological cofactors). With quantum contributions to the reorganization energy on the scale of hundreds of meV,[13,22,59,78] substantial energy dissipation is required to avoid charge recombination, and the regime of high quantum yields with lower-energy electron-hole pairs optimizes the overall energy efficiency. As we made may assumptions in formulating our model, further insights into the kinetic and thermodynamic compromises at play in biological reaction centers may be accessible with more granular theoretical treatments (e.g., explicit physical models of the outer-sphere reorganization and solvation,[25,73,98,99] dynamical fluctuations,[100-102] multiple distinct quantum modes,[31,85] etc.).

Our results inform the design of systems that are not limited by constraints to physiological cofactors, such as synthetic multi-step ET architectures[39-47] and *de novo* protein structures that bind abiological energy-transducing cofactors.[103-105] We find that high quantum yields and low energy dissipation can be simultaneously realized for multistep ET if: (i) the CR pathways from intermediate CS states are uncoupled from high-frequency vibrations (i.e., CR pathways are effectively slowed by the Marcus-inverted effect or by orbital symmetry effects); (ii) the cofactors are held at an intermediate distance (ca. 3 to 8 Å distances for the simple model studied here) to

limit charge recombination. Fulfilling these criteria and tuning the additional factors explored here (cofactor diameter, wavefunction decay rate, etc.) may provide alternative avenues to advance technologies beyond the ~30% energy efficiency achieved during energy conversion in natural RCs.

ASSOCIATED CONTENT

Supporting Information

The Supporting Information is available free of charge at DOI:XXXX and includes additional theoretical details and simulation results.

Data and Code Availability

The data discussed in this work and the codes used to generate them are available[106] free of charge at the repository provided in Ref. 106.

AUTHOR INFORMATION

Corresponding Author

David N. Beratan - Department of Chemistry, Duke University, Durham, North Carolina, 27708, United States; Department of Physics, Duke University, Durham, North Carolina, 27708, United States; Department of Biochemistry, Duke University, Durham, North Carolina, 27710, United States; orcid.org/0000-0003-4758-8676; Email: david.beratan@duke.edu

Authors

Jonathan D. Schultz - Department of Chemistry, Duke University, Durham, North Carolina 27708, United States; orcid.org/0000-0002-3386-5460

Kelsey A. Parker - Department of Chemistry, Duke University, Durham, North Carolina 27708, United States; orcid.org/0000-0002-9176-3681

Michael J. Therien - Department of Chemistry, Duke University, Durham, North Carolina 27708, United States; orcid.org/0000-0003-4876-0036

NOTES

The authors declare no competing financial interest.

ACKNOWLEDGMENTS

This material is based upon work supported by the National Science Foundation Grant CHE-2109020. J.D.S. gratefully acknowledges support from an Arnold O. Beckman Postdoctoral Fellowship in the Chemical Sciences (dx.doi.org/10.13039/100000997).

REFERENCES

(1) Kirmaier, C.; Holten, D. Primary photochemistry of reaction centers from the photosynthetic purple bacteria. *Photosynth. Res.* **1987**, *13* (3), 225-260

(2) Feher, G.; Allen, J. P.; Okamura, M. Y.; Rees, D. C. Structure and function of bacterial photosynthetic reaction centres. *Nature* **1989**, *339* (6220), 111-116

(3) Zinth, W.; Wachtveitl, J. The first picoseconds in bacterial photosynthesis--ultrafast electron transfer for the efficient conversion of light energy. *Chem. Phys. Chem.* **2005**, *6* (5), 871-880

(4) Markvart, T. Light harvesting for quantum solar energy conversion. *Prog. Quant. Electron.* **2000**, *24* (3-4), 107-186

(5) Moser, C. C.; Keske, J. M.; Warncke, K.; Farid, R. S.; Dutton, P. L. Nature of biological electron transfer. *Nature* **1992**, *355* (6363), 796-802

(6) Moser, C. C.; Page, C. C.; Cogdell, R. J.; Barber, J.; Wraight, C. A.; Dutton, P. L. Length, time, and energy scales of photosystems. *Adv. Protein Chem.* **2003**, *63*, 71-109

(7) Moser, C. C.; Dutton, P. L. *Application of marcus theory to photosystem I electron transfer*; 2006.

(8) Blankenship, R. E. *Molecular mechanisms of photosynthesis*; John Wiley & Sons, 2021.

(9) Okamura, M.; Paddock, M.; Graige, M.; Feher, G. Proton and electron transfer in bacterial reaction centers. *Biochim Biophys Acta Bioenerg.* **2000**, *1458* (1), 148-163

(10) Holzapfel, W.; Finkele, U.; Kaiser, W.; Oesterhelt, D.; Scheer, H.; Stilz, H. U.; Zinth, W. Initial Electron-Transfer in the Reaction Center from Rhodobacter-Sphaeroides. *Proc. Natl. Acad. Sci. U.S.A.* **1990**, *87* (13), 5168-5172

(11) Milano, F.; Agostiano, A.; Mavelli, F.; Trotta, M. Kinetics of the quinone binding reaction at the QB site of reaction centers from the purple bacteria Rhodobacter sphaeroides reconstituted in liposomes. *Eur. J. Biochem.* **2003**, *270* (23), 4595-4605

(12) Stowell, M.; McPhillips, T.; Rees, D.; Soltis, S.; Abresch, E.; Feher, G. Light-induced structural changes in photosynthetic reaction center: implications for mechanism of electron-proton transfer. *Science* **1997**, *276* (5313), 812-816

(13) Gunner, M.; Dutton, P. L. Temperature and -ΔG° dependence of the electron transfer from BPh^- to Q_A in reaction center protein from Rhodobacter sphaeroides with different quinones as Q_A. *J. Am. Chem. Soc.* **1989**, *111* (9), 3400-3412

(14) Marcus, R. A. Electron transfer reactions in chemistry: theory and experiment (Nobel lecture). *Angew. Chem., Int. Ed. Engl.* **1993**, *32* (8), 1111-1121

(15) Rutherford, A. W.; Osyczka, A.; Rappaport, F. Back-reactions, short-circuits, leaks and other energy wasteful reactions in biological electron transfer: redox tuning to survive life in O(2). *FEBS Lett.* **2012**, *586* (5), 603-616

(16) Makita, H.; Hastings, G. Inverted-region electron transfer as a mechanism for enhancing photosynthetic solar energy conversion efficiency. *Proc. Natl. Acad. Sci. U.S.A.* **2017**, *114* (35), 9267-9272

(17) Marcus, R. On the theory of electrochemical and chemical electron transfer processes. *Can. J. Chem.* **1959**, *37*, 155

(18) Marcus, R. A.; Sutin, N. Electron transfers in chemistry and biology. *Biochim. Biophys. Acta* **1985**, *811*, 265-322

(19) Marcus, R. A. Chemical and electrochemical electron-transfer theory. *Annu. Rev. Phys. Chem.* **1964**, *15*, 155

(20) Gray, H. B.; Winkler, J. R. Electron tunneling through proteins. *Q. Rev. Biophys.* **2003**, *36* (3), 341-372

(21) Zhang, X.; Gunner, M. Affinity and activity of non-native quinones at the QB site of bacterial photosynthetic reaction centers. *Photosynth. Res.* **2014**, *120*, 181-196

(22) Gunner, M.; Robertson, D. E.; Dutton, P. L. Kinetic studies on the reaction center protein from Rhodopseudomonas sphaeroides: the temperature and free energy dependence of electron transfer between various quinones in the QA site and the oxidized bacteriochlorophyll dimer. *J. Phys. Chem.* **1986**, *90* (16), 3783-3795

(23) Kirmaier, C.; Holten, D.; Parson, W. W. Temperature and detection-wavelength dependence of the picosecond electron-transfer kinetics measured in Rhodopseudomonas sphaeroides reaction centers. Resolution of new spectral and kinetic components in the primary charge-separation process. *Biochim. Biophys. Acta, Bioenerg.* **1985**, *810* (1), 33-48

(24) Volk, M.; Aumeier, G.; Langenbacher, T.; Feick, R.; Ogrodnik, A.; Michel-Beyerle, M.-E. Energetics and mechanism of primary charge separation in bacterial photosynthesis. A comparative study on reaction centers of Rhodobacter sphaeroides and Chloroflexus aurantiacus. *J. Phys. Chem. B* **1998**, *102* (4), 735-751

(25) Matyushov, D. V. Reorganization energy of electron transfer. *Phys. Chem. Chem. Phys.* **2023**, *25* (11), 7589-7610

(26) Amashukeli, X.; Gruhn, N. E.; Lichtenberger, D. L.; Winkler, J. R.; Gray, H. B. Inner-Sphere Electron-Transfer Reorganization Energies of Zinc Porphyrins. *J. Am. Chem. Soc.* **2004**, *126* (47), 15566-15571

(27) Gruhn, N. E.; da Silva Filho, D. A.; Bill, T. G.; Malagoli, M.; Coropceanu, V.; Kahn, A.; Brédas, J.-L. The Vibrational Reorganization Energy in Pentacene: Molecular Influences on Charge Transport. *J. Am. Chem. Soc.* **2002**, *124* (27), 7918-7919

(28) Amashukeli, X.; Winkler, J. R.; Gray, H. B.; Gruhn, N. E.; Lichtenberger, D. L. Electron-Transfer Reorganization Energies of Isolated Organic Molecules. *J. Phys. Chem. A* **2002**, *106* (33), 7593-7598

(29) Yang, C.-H.; Wang, C.-I.; Wang, Y.-S.; Hsu, C.-P. Non-negligible Outer-Shell Reorganization Energy for Charge Transfer in Nonpolar Systems. *J. Chem. Theory Comput.* **2024**, *20* (16), 6981-6991

(30) Lavergne, J.; Joliot, P. Dissipation in bioenergetic electron transfer chains. *Photosynth. Res.* **1996**, *48* (1), 127-138

(31) Siplivy, N. B.; Feskov, S. V.; Ivanov, A. I. Quantum yield and energy efficiency of photoinduced intramolecular charge separation. *J. Chem. Phys.* **2020**, *153* (4), 044301

(32) Noy, D.; Moser, C. C.; Dutton, P. L. Design and engineering of photosynthetic light-harvesting and electron transfer using length, time, and energy scales. *Biochim. Biophys. Acta, Bioenerg.* **2006**, *1757* (2), 90-105

(33) Page, C. C.; Moser, C. C.; Chen, X.; Dutton, P. L. Natural engineering principles of electron tunnelling in biological oxidation–reduction. *Nature* **1999**, *402* (6757), 47-52

(34) Noy, D. Natural photosystems from an engineer's perspective: length, time, and energy scales of charge and energy transfer. *Photosynth. Res.* **2008**, *95* (1), 23-35

(35) Gust, D.; Moore, T. A. Mimicking photosynthesis. *Science* **1989**, *244* (4900), 35-41

(36) Wasielewski, M. R. Photoinduced electron transfer in supramolecular systems for artificial photosynthesis. *Chem. Rev.* **1992**, *92* (3), 435-461

(37) Fukuzumi, S.; Lee, Y.-M.; Nam, W. Bioinspired artificial photosynthesis systems. *Tetrahedron* **2020**, *76* (14), 131024

(38) Llansola-Portoles, M. J.; Gust, D.; Moore, T. A.; Moore, A. L. Artificial photosynthetic antennas and reaction centers. *C. R. Chim.* **2017**, *20* (3), 296-313

(39) Palacios, R. E.; Kodis, G.; Gould, S. L.; De La Garza, L.; Brune, A.; Gust, D.; Moore, T. A.; Moore, A. L. Artificial Photosynthetic Reaction Centers: Mimicking Sequential Electron and Triplet-Energy Transfer. *ChemPhysChem* **2005**, *6* (11), 2359-2370

(40) Cordes, M.; Köttgen, A.; Jasper, C.; Jacques, O.; Boudebous, H.; Giese, B. Influence of amino acid side chains on long-distance electron transfer in peptides: electron hopping via "stepping stones". *Angew. Chem. Int. Ed.* **2008**, *47* (18), 3461-3463

(41) Yanagisawa, K.; Morita, T.; Kimura, S. Efficient photocurrent generation by self-assembled monolayers composed of 310-helical peptides carrying linearly spaced Naphthyl groups at the side chains. *J. Am. Chem. Soc.* **2004**, *126* (40), 12780-12781

(42) Ricks, A. B.; Brown, K. E.; Wenninger, M.; Karlen, S. D.; Berlin, Y. A.; Co, D. T.; Wasielewski, M. R. Exponential distance dependence of photoinitiated stepwise electron transfer in donor–bridge–acceptor molecules: implications for wirelike behavior. *J. Am. Chem. Soc.* **2012**, *134* (10), 4581-4588

(43) Wilson, T. M.; Zeidan, T. A.; Hariharan, M.; Lewis, F. D.; Wasielewski, M. R. Electron hopping among cofacially stacked perylenediimides assembled by using DNA hairpins. *Angew. Chem. Int. Ed* **2010**, *49* (13), 2385-2388

(44) Mes, G. F.; Van Ramesdonk, H. J.; Verhoeven, J. W. Photoinduced electron transfer in polychromophoric systems. 2. Protonation directed switching between tri-and bichromophoric interaction. *J. Am. Chem. Soc.* **1984**, *106* (5), 1335-1340

(45) Gust, D.; Moore, T. A.; Moore, A. L.; Lee, S.-J.; Bittersmann, E.; Luttrull, D. K.; Rehms, A. A.; DeGraziano, J. M.; Ma, X. C.; Gao, F. Efficient multistep photoinitiated electron transfer in a molecular pentad. *Science* **1990**, *248* (4952), 199-201

(46) Gust, D.; Moore, T. A.; Moore, A. L.; Barrett, D.; Harding, L. O.; Makings, L. R.; Liddell, P. A.; De Schryver, F.; Van der Auweraer, M. Photoinitiated charge separation in a carotenoid-porphyrin-diquinone tetrad: enhanced quantum yields via multistep electron transfers. *J. Am. Chem. Soc.* **1988**, *110* (1), 321-323

(47) Imahori, H.; Sekiguchi, Y.; Kashiwagi, Y.; Sato, T.; Araki, Y.; Ito, O.; Yamada, H.; Fukuzumi, S. Long-Lived Charge-Separated State Generated in a Ferrocene–meso, meso-Linked Porphyrin Trimer–Fullerene Pentad with a High Quantum Yield. *Chem. Eur. J.* **2004**, *10* (13), 3184-3196

(48) Guldi, D. M.; Imahori, H.; Tamaki, K.; Kashiwagi, Y.; Yamada, H.; Sakata, Y.; Fukuzumi, S. A molecular tetrad allowing efficient energy storage for 1.6 s at 163 K. *J. Phys. Chem. A* **2004**, *108* (4), 541-548

(49) Imahori, H.; Guldi, D. M.; Tamaki, K.; Yoshida, Y.; Luo, C.; Sakata, Y.; Fukuzumi, S. Charge separation in a novel artificial photosynthetic reaction center lives 380 ms. *J. Am. Chem. Soc.* **2001**, *123* (27), 6617-6628

(50) Jortner, J. Temperature dependent activation energy for electron transfer between biological molecules. *J. Chem. Phys.* **1976**, *64* (12), 4860-4867

(51) Jortner, J.; Bixon, M. Intramolecular vibrational excitations accompanying solvent-controlled electron transfer reactions. *J. Chem. Phys.* **1988**, *88*, 167–170

(52) Liang, N., Miller, J. R., Closs, G. L. Temperature-Independent Long-Range Electron Transfer Reactions in the Marcus Inverted Region. *J. Am. Chem. Soc.* **1990**, *112*, 5353-5354

(53) Turro, C.; Zaleski, J. M.; Karabatsos, Y. M.; Nocera, D. G. Bimolecular electron transfer in the Marcus inverted region. *J. Am. Chem. Soc.* **1996**, *118* (25), 6060-6067

(54) Closs, G. L.; Calcaterra, L. T.; Green, N. J.; Penfield, K. W.; Miller, J. R. Distance, Stereoelectronic Effects, and the Marcus Inverted Region in Intramolecular Electron Transfer in Organic Radical Anions. *J. Phys. Chem.* **1986**, *90* (16), 3673-3683

(55) Yang, L. N.; Zhou, H. Y.; Sun, P. P.; Chen, S. L.; Li, Z. S. A promising candidate with D-A-A-A architecture as an efficient sensitizer for dye-sensitized solar cells. *ChemPhysChem* **2015**, *16* (3), 601-606

(56) Gust, D.; Moore, T. A.; Moore, A. L.; Makings, L. R.; Seely, G. R.; Ma, X.; Trier, T. T.; Gao, F. A carotenoid-diporphyrin-quinone model for photosynthetic multistep electron and energy transfer. *J. Am. Chem. Soc.* **1988**, *110* (22), 7567-7569

(57) Cao, Y.; Zhang, B. W.; Qian, W. Y.; Wang, X. D.; Bai, J. W.; Xiao, X. R.; Jia, J. G.; Xu, J. W. An artificial photosynthesis porphyrin tetrad molecule for photoelectric conversion. *Sol. Energy Mater. Sol. Cells* **1995**, *38* (1-4), 139-155

(58) Closs, G. L.; Miller, J. R. Intramolecular long-distance electron transfer in organic molecules. *Science* **1988**, *240* (4851), 440-447

(59) Bixon, M.; Jortner, J. Non-Arrhenius temperature dependence of electron-transfer rates. *J. Phys. Chem.* **1991**, *95* (5), 1941-1944

(60) Hopfield, J. J. Electron transfer between biological molecules by thermally activated tunneling. *Proc. Natl. Acad. Sci. U.S.A.* **1974**, *71*, 3640-3644

(61) Prytkova, T. R.; Kurnikov, I. V.; Beratan, D. N. Coupling coherence distinguishes structure sensitivity in protein electron transfer. *Science* **2007**, *315* (5812), 622-625

(62) Winkler, J. R.; Gray, H. B.; Prytkova, T. R.; Kurnikov, I. V.; Beratan, D. N. *Electron transfer through proteins*; 2005.

(63) Lewis, F. D.; Liu, J.; Weigel, W.; Rettig, W.; Kurnikov, I. V.; Beratan, D. N. Donor-bridge-acceptor energetics determine the distance dependence of electron tunneling in DNA. *Proc. Natl. Acad. Sci. U.S.A.* **2002**, *99* (20), 12536-12541

(64) Onuchic, J. N.; Beratan, D. N.; Winkler, J. R.; Gray, H. B. Pathway analysis of protein electron-transfer reactions. *Annu. Rev. Biophys. Biomol. Struct.* **1992**, *21* (1), 349-377

(65) Beratan, D. N.; Betts, J. N.; Onuchic, J. N. Protein Electron Transfer Rates Set by the Bridging Secondary and Tertiary Structure. *Science* **1991**, *252* (5010), 1285-1288

(66) Onuchic, J. N.; Beratan, D. N. A predictive theoretical model for electron tunneling pathways in proteins. *J. Chem. Phys.* **1990**, *92* (1), 722-733

(67) Jones, M. L.; Kurnikov, I. V.; Beratan, D. N. The Nature of Tunneling Pathway and Average Packing Density Models for Protein-Mediated Electron Transfer. *J. Phys. Chem. A* **2002**, *106* (10), 2002-2006

(68) Beratan, D. N.; Onuchic, J. N.; Hopfield, J. J. Electron tunneling through covalent and noncovalent pathways in proteins. *J. Chem. Phys.* **1987**, *86* (8), 4488

(69) Beratan, D. N.; Skourtis, S. S.; Balabin, I. A.; Balaeff, A.; Keinan, S.; Venkatramani, R.; Xiao, D. Steering electrons on moving pathways. *Acc. Chem. Res.* **2009**, *42* (10), 1669-1678

(70) Nagarajan, V.; Parson, W.; Davis, D.; Schenck, C. Kinetics and free energy gaps of electron-transfer reactions in Rhodobacter sphaeroides reaction centers. *Biochem.* **1993**, *32* (46), 12324-12336

(71) Onuchic, J. N.; Beratan, D. N. Molecular Bridge Effects on Distant Charge Tunneling. *J. Am. Chem. Soc.* **1987**, *109* (22), 6771-6778

(72) Page, C. C.; Moser, C. C.; Dutton, P. L. Mechanism for electron transfer within and between proteins. *Curr. Opin. Chem. Biol.* **2003**, *7* (5), 551-556

(73) Matyushov, D. V.; Newton, M. D. Thermodynamics of reactions affected by medium reorganization. *J. Phys. Chem. B* **2018**, *122* (51), 12302-12311

(74) Ghorai, P. K.; Matyushov, D. V. Solvent reorganization entropy of electron transfer in polar solvents. *J. Phys. Chem. A* **2006**, *110* (28), 8857-8863

(75) Milischuk, A. A.; Matyushov, D. V.; Newton, M. D. Activation entropy of electron transfer reactions. *Chem. Phys.* **2006**, *324* (1), 172-194

(76) Dutton, P. L.; Moser, C. C. Quantum biomechanics of long-range electron transfer in protein: hydrogen bonds and reorganization energies. *Proc. Natl. Acad. Sci. U.S.A.* **1994**, *91* (22), 10247-10250

(77) Rafiq, S.; Scholes, G. D. From Fundamental Theories to Quantum Coherences in Electron Transfer. *J. Am. Chem. Soc.* **2019**, *141* (2), 708-722

(78) Borrelli, R.; Di Donato, M.; Peluso, A. Role of intramolecular vibrations in long-range electron transfer between pheophytin and ubiquinone in bacterial photosynthetic reaction centers. *Biophys. J.* **2005**, *89* (2), 830-841

(79) Terai, K.; Yuly, J. L.; Zhang, P.; Beratan, D. N. Correlated particle transport enables biological free energy transduction. *Biophys. J.* **2023**, *122* (10), 1762-1771

(80) Barbara, P. F.; Meyer, T. J.; Ratner, M. A. Contemporary Issues in Electron Transfer Research. *J. Phys. Chem.* **1996**, *100* (31), 13148-13168

(81) Miller, J. R.; Calcaterra, L. T.; Closs, G. L. Intramolecular long-distance electron transfer in radical anions. The effects of free energy and solvent on the reaction rates. *J. Am. Chem. Soc.* **1984**, *106* (10), 3047-3049

(82) Alric, J.; Lavergne, J.; Rappaport, F.; Verméglio, A.; Matsuura, K.; Shimada, K.; Nagashima, K. V. P. Kinetic Performance and Energy Profile in a Roller Coaster Electron Transfer Chain: A Study of Modified Tetraheme-Reaction Center Constructs. *J. Am. Chem. Soc.* **2006**, *128* (12), 4136-4145

(83) Wang, J.; Ding, T.; Gao, K.; Wang, L.; Zhou, P.; Wu, K. Marcus inverted region of charge transfer from low-dimensional semiconductor materials. *Nat. Commun.* **2021**, *12* (1), 6333

(84) Creutz, C.; Sutin, N. Vestiges of the "inverted region" for highly exergonic electron-transfer reactions. *J. Am. Chem. Soc.* **1977**, *99* (1), 241-243

(85) Chaudhuri, S.; Hedström, S.; Méndez-Hernández, D. D.; Hendrickson, H. P.; Jung, K. A.; Ho, J.; Batista, V. S. Electron Transfer Assisted by Vibronic Coupling from Multiple Modes. *J. Chem. Theory Comput.* **2017**, *13* (12), 6000-6009

(86) Siders, P.; Marcus, R. A. Quantum effects for electron-transfer reactions in the" inverted region". *J. Am. Chem. Soc.* **1981**, *103* (4), 748-752

(87) Åkesson, E.; Walker, G. C.; Barbara, P. F. Dynamic solvent effects on electron transfer rates in the inverted regime: Ultrafast studies on the betaines. *J. Chem. Phys.* **1991**, *95* (6), 4188-4194

(88) Fox, L. S.; Kozik, M.; Winkler, J. R.; Gray, H. B. Gaussian Free-Energy Dependence of Electron-Transfer Rates in Iridium Complexes. *Science* **1990**, *247* (4946), 1069-1071

(89) Ward, A. J.; Ruseckas, A.; Kareem, M. M.; Ebenhoch, B.; Serrano, L. A.; Al-Eid, M.; Fitzpatrick, B.; Rotello, V. M.; Cooke, G.; Samuel, I. D. The impact of driving force on electron transfer rates in photovoltaic donor–acceptor blends. *Adv. Mater.* **2015**, *27* (15), 2496-2500

(90) Coffey, D. C.; Larson, B. W.; Hains, A. W.; Whitaker, J. B.; Kopidakis, N.; Boltalina, O. V.; Strauss, S. H.; Rumbles, G. An optimal driving force for converting excitons into free carriers in excitonic solar cells. *J. Phys. Chem. C* **2012**, *116* (16), 8916-8923

(91) Coropceanu, V.; Malagoli, M.; da Silva Filho, D. A.; Gruhn, N. E.; Bill, T. G.; Brédas, J. L. Hole- and Electron-Vibrational Couplings in Oligoacene Crystals: Intramolecular Contributions. *Phys. Rev. Lett.* **2002**, *89* (27), 275503

(92) Wu, C.-C.; Li, E. Y.; Chou, P.-T. Reducing the internal reorganization energy via symmetry controlled π-electron delocalization. *Chem. Sci.* **2022**, *13* (24), 7181-7189

(93) Rawson, J.; Angiolillo, P. J.; Therien, M. J. Extreme electron polaron spatial delocalization in π-conjugated materials. *Proc. Natl. Acad. Sci. U.S.A.* **2015**, *112* (45), 13779-13783

(94) Susumu, K.; Frail, P. R.; Angiolillo, P. J.; Therien, M. J. Conjugated chromophore arrays with unusually large hole polaron delocalization lengths. *J. Am. Chem. Soc.* **2006**, *128* (26), 8380-8381

(95) Sigfridsson, E.; Olsson, M. H.; Ryde, U. Inner-sphere reorganization energy of iron− sulfur clusters studied with theoretical methods. *Inorg. Chem.* **2001**, *40* (11), 2509-2519

(96) Beddard, G. Excitations and excitons in photosystem I. *Philos. Transact. A Math. Phys. Eng. Sci.* **1998**, *356* (1736), 421-448

(97) Beddard, G. S.; Carlin, S. E.; Porter, G. Concentration quenching of chlorophyll fluorescence in bilayer lipid vesicles and liposomes. *Chem. Phys. Lett.* **1976**, *43* (1), 27-32

(98) Rips, I.; Jortner, J. Dynamic solvent effects on outer-sphere electron transfer. *J. Chem. Phys.* **1987**, *87* (4), 2090-2104

(99) Van Voorhis, T.; Kowalczyk, T.; Kaduk, B.; Wang, L.-P.; Cheng, C.-L.; Wu, Q. The diabatic picture of electron transfer, reaction barriers, and molecular dynamics. *Annu. Rev. Phys. Chem.* **2010**, *61* (1), 149-170

(100) Parker, K. A.; Beratan, D. N. Undulating Free Energy Landscapes Buffer Redox Chains from Environmental Fluctuations. *J. Phys. Chem. B* **2024**,

(101) Zhang, Y.; Liu, C.; Balaeff, A.; Skourtis, S. S.; Beratan, D. N. Biological charge transfer via flickering resonance. *Proc. Natl. Acad. Sci. U.S.A.* **2014**, *111* (28), 10049-10054

(102) Skourtis, S. S.; Waldeck, D. H.; Beratan, D. N. Fluctuations in biological and bioinspired electron-transfer reactions. *Annu. Rev. Phys. Chem.* **2010**, *61* (1), 461-485

(103) Polizzi, N. F.; Eibling, M. J.; Perez-Aguilar, J. M.; Rawson, J.; Lanci, C. J.; Fry, H. C.; Beratan, D. N.; Saven, J. G.; Therien, M. J. Photoinduced Electron Transfer Elicits a Change in the Static Dielectric Constant of a de Novo Designed Protein. *J. Am. Chem. Soc.* **2016**, *138* (7), 2130-2133

(104) Korendovych, I. V.; Senes, A.; Kim, Y. H.; Lear, J. D.; Fry, H. C.; Therien, M. J.; Blasie, J. K.; Walker, F. A.; DeGrado, W. F. De Novo Design and Molecular Assembly of a Transmembrane Diporphyrin-Binding Protein Complex. *J. Am. Chem. Soc.* **2010**, *132* (44), 15516-15518

(105) Bender, G. M.; Lehmann, A.; Zou, H.; Cheng, H.; Fry, H. C.; Engel, D.; Therien, M. J.; Blasie, J. K.; Roder, H.; Saven, J. G.; DeGrado, W. F. De Novo Design of a Single-Chain Diphenylporphyrin Metalloprotein. *J. Am. Chem. Soc.* **2007**, *129* (35), 10732-10740

(106) Schultz, J. D.; Parker, K. A.; Therien, M. J.; Beratan, D. N. *Code and data repository for ET chain energy efficiency manuscript.*; 2024. DOI: DOI (Zenodo) pending...

TOC Graphic